

THE OFFICIAL MAGAZINE OF THE OCEANOGRAPHY SOCIETY

Oceanography

CITATION

Horstmann, J., C. Wackerman, S. Falchetti, and S. Maresca. 2013. Tropical cyclone winds retrieved from synthetic aperture radar. *Oceanography* 26(2):46–57, <http://dx.doi.org/10.5670/oceanog.2013.30>.

DOI

<http://dx.doi.org/10.5670/oceanog.2013.30>

COPYRIGHT

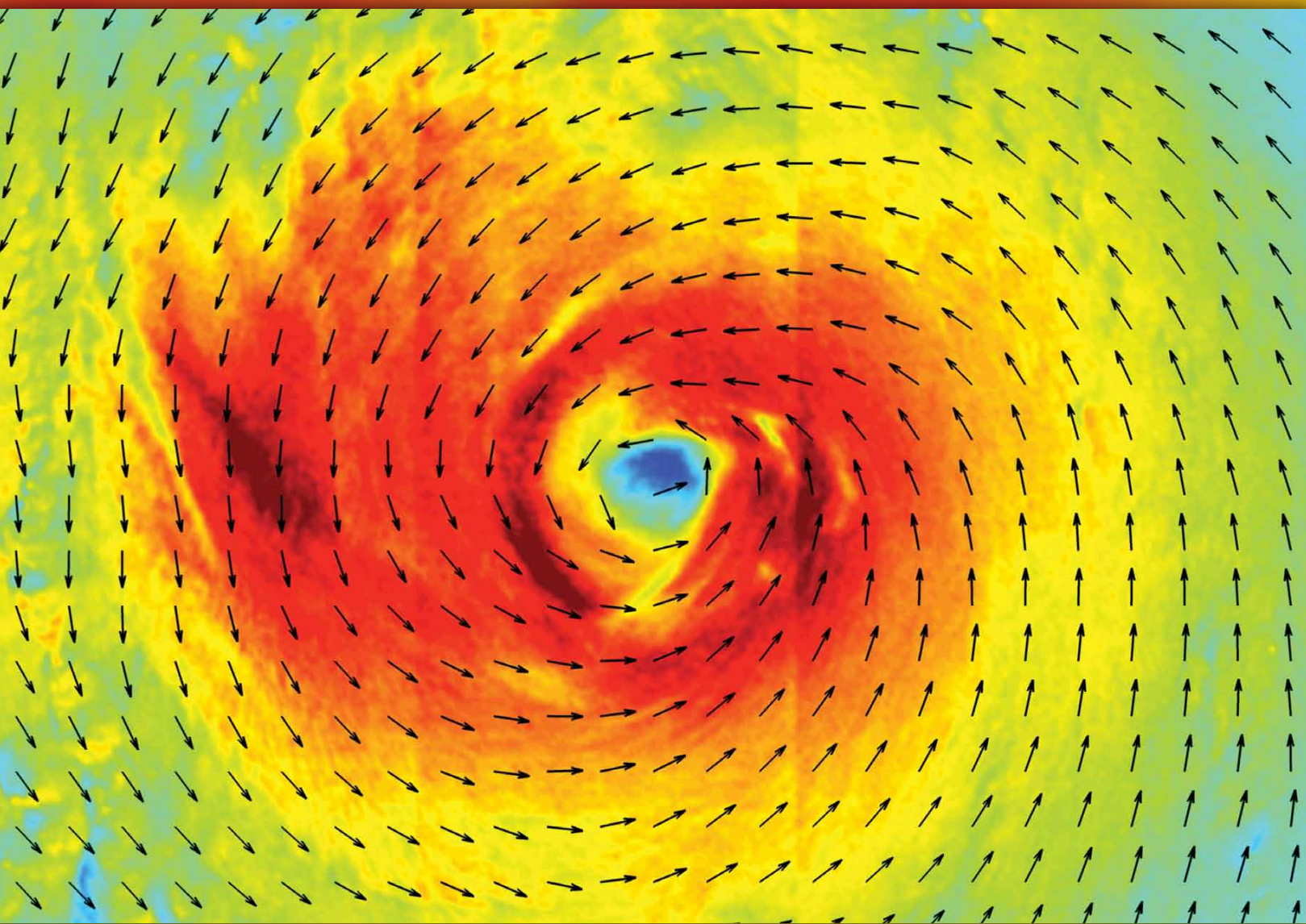
This article has been published in *Oceanography*, Volume 26, Number 2, a quarterly journal of The Oceanography Society. Copyright 2013 by The Oceanography Society. All rights reserved.

USAGE

Permission is granted to copy this article for use in teaching and research. Republication, systematic reproduction, or collective redistribution of any portion of this article by photocopy machine, reposting, or other means is permitted only with the approval of The Oceanography Society. Send all correspondence to: info@tos.org or The Oceanography Society, PO Box 1931, Rockville, MD 20849-1931, USA.

TROPICAL CYCLONE WINDS RETRIEVED FROM SYNTHETIC APERTURE RADAR

BY JOCHEN HORSTMANN, CHRISTOPHER WACKERMAN,
SILVIA FALCHETTI, AND SALVATORE MARESCA



RADARSAT-2 ScanSAR retrieved wind field
of Hurricane Earl acquired on September 2,
2010, at 22:59 UTC at cross-polarization.

ABSTRACT. This paper describes algorithms used to retrieve high-resolution wind fields in tropical cyclone conditions from synthetic aperture radar (SAR) data acquired at C-band with either co-polarization or cross-polarization. Wind directions are estimated from the orientation of wind-induced streaks visible in SAR images using a simple tropical cyclone flow field. Wind speeds are retrieved from the normalized radar cross section taking into account imaging geometry and SAR-retrieved wind direction using a geophysical model function. The algorithms are validated by comparing outputs to a set of SAR images acquired under tropical cyclone conditions. The simulated wind fields are compared to co-located results from the QuikSCAT scatterometer as well as to wind speeds measured by the Stepped Frequency Microwave Radiometer (SFMR) during reconnaissance flights through individual storms. Comparison of QuikSCAT winds to SAR co-polarization data shows that winds can be retrieved with a root mean square error of 17.6° for wind directions and 4.6 m s^{-1} for wind speeds. Comparison of SAR wind speeds to SFMR data result in a root mean square error of 5.7 m s^{-1} for co-polarization data and 3.8 m s^{-1} for cross-polarization data. SAR cross-polarization data are significantly better suited for SAR wind retrieval under tropical cyclone conditions at wind speeds above approximately 20 m s^{-1} .

INTRODUCTION

Observation of tropical cyclones (TCs) is vital because these systems are capable of extreme destruction when approaching the coast or making landfall. The ability to accurately predict their behavior, especially with respect to strength and propagation direction and speed, is an essential component of providing accurate evacuation information and effective allocation of remediation resources. In the past decade, microwave sensors such as scatterometers, radiometers, and altimeters have been shown to offer safe and cost-effective possibilities for measuring TC parameters and to provide more accurate initial conditions for model predictions. They permit a better understanding of the storms primarily because they can collect data independent of daylight and their signals can penetrate the extreme cloud cover

associated with TCs (Katsaros et al., 2002). In the last decade, there has been substantial interest in synthetic aperture radar (SAR) because of its high resolution ($< 100 \text{ m}$) and large spatial coverage ($\approx 500 \text{ km}$ wide swath along the orbit). Katsaros et al. (2000) show that SAR images display storm structure in great detail, and they discuss some of the potential of these data for extraction of various storm parameters.

In the last decade, C-band SAR data of TCs have been collected on a regular basis at either vertical (V) or horizontal (H) polarization in transmit and receive—the so called co-polarization (co-pol) mode. These data have been investigated intensively, particularly with respect to ocean surface wind and wave retrieval. Horstmann et al. (2005) showed the capabilities and limitations of measuring quantitative

hurricane-force surface winds using the well-validated geophysical model function (GMF) CMOD5. Shen et al. (2009) show that wind speed error increases significantly for high wind speeds due to the decrease in sensitivity of a normalized radar cross section (NRCS) with increasing wind speed. Reppucci et al. (2010) addressed this sensitivity issue by using SAR-retrieved wind fields at low to moderate winds to adjust a simple numerical model for TCs and estimating storm intensities. Recently, cross-polarization (cross-pol) SAR images, which are acquired at H-pol in transmit and V-pol in receive (HV-pol), or vice versa (VH-pol), have been investigated for possible use in wind speed retrieval. These studies suggest that the relation between wind speed and NRCS is independent of incidence angle and wind direction and that there is no saturation effect at high wind speeds (Hwang et al., 2010; Vachon and Wolfe, 2011; Zhang et al., 2011). Most recent results using SAR cross-pol data indicate they can overcome the limitations of co-pol SAR data with respect to wind speeds in TCs (van Zedelhoff et al., 2013).

In this paper, we introduce and validate the capabilities of C-band SARs for wind retrieval under TC conditions using co-located winds obtained from the scatterometer aboard QuikSCAT as well as measurements obtained by Stepped Frequency Microwave Radiometers (SFMRs) aboard C-130 aircraft. We then introduce the data used in this investigation and describe the SAR wind retrieval algorithms for C-band SAR considering the different

polarization pairs. We then compare the SAR-retrieved wind fields to QuikSCAT and SFMR data. Finally, we present conclusions and perspectives for future work.

“ THIS STUDY SHOWS THAT IT IS POSSIBLE TO GENERATE USEFUL INFORMATION ABOUT THE WIND FIELD WITHIN A TYPHOON FROM SAR IMAGERY IN EITHER CO-POL OR CROSS-POL MODES THAT COULD BE USED TO INITIALIZE MODEL PREDICTIONS AND POTENTIALLY GENERATE IMPROVED PERFORMANCE. ”

DATA

The SAR data used in this investigation were acquired by the Canadian satellites RADARSAT-1 (1997 to 2013) and RADARSAT-2 (since 2007) in the ScanSAR Wide mode A (SCWA). In this mode, the SAR instrument uses four single beams, with each beam selected sequentially, enabling data collection from a wider swath. The nominal ScanSAR image covers approximately 500 km along the swath with a resolution of 100 m in azimuth (flight direction) and between 160 m and 72 m from near to far range (incidence angles between 20° and 49°). RADARSAT-1 was only capable of acquiring SAR data at C-band with HH-pol, while RADARSAT-2 enables acquisition of SAR data at dual-pol, where the SAR transmits with either V-pol or H-pol and receives the backscatter at both polarizations. The dual-pol acquisitions result in two individual SAR images, where one is recorded at

co-pol (HH or VV) and the other at cross-pol (HV or VH).

A significant issue with radars collecting at multiple polarizations is antenna isolation performance, which

if too low leads to contributions from the other channel in the NRCS measurements (cross talk). In the case of RADARSAT-2 ScanSAR data, the isolation is better than -32 dB and mainly affects NRCS collected at small incidence angles (Touzi et al., 2010). In addition to cross talk, the data acquired at cross-pol are strongly dependent on the noise floor of the instrument. In the case of RADARSAT-2 SCWA data, the noise floor is approximately -28 dB \pm 2 dB, which is on the order of the NRCS from the ocean surface under low to moderate wind conditions. For this reason, ScanSAR cross-pol data have been

corrected for the noise floor prior to wind speed retrieval (recent work of the authors and colleagues).

Data from the SeaWinds scatterometer on QuikSCAT (1999 to 2009) were compared with SAR-retrieved wind fields. The SeaWinds scatterometer is a spaceborne radar that operates a dual-beam antenna at Ku-band (13.4 GHz), with both VV- and HH-pol to measure the NRCS at fixed incidence angles of 46° and 54°. While the spacecraft proceeds in orbit, the antenna rotates and scans a swath width of 1,800 km with a resolution of approximately 25 km. Because the outer 200 km of the swath only records measurements from the higher incidence angle beam, the wind field is restricted to the middle 1,600 km of the swath. The wind retrievals are calibrated to the equivalent neutral-stability winds at a reference height of 10 m above the sea surface. Comparison of QuikSCAT wind speeds to data acquired by Chelton and Freilich (2005) from buoys of the National Data Buoy Center resulted in a root mean square (rms) error of 1.2 m s⁻¹ with a 0.11 m s⁻¹ bias. Wind directions have shown a large error at low wind speeds, which reduces to 14° at wind speeds over 6 m s⁻¹.

ScanSAR winds retrieved at co- and cross-pol simultaneously were compared with wind speeds retrieved from the SFMR aboard the C-130 aircraft. The SFMR was specifically developed to

Jochen Horstmann (jocholo@gmail.com) was a scientist at the Centre for Maritime Research and Experimentation, La Spezia, Italy, and is now Department Head, Institute of Coastal Research, Helmholtz-Zentrum Geesthacht, Germany. **Christopher Wackerman** is a scientist at General Dynamics Advanced Information Systems, Ypsilanti, MI, USA. **Silvia Falchetti** is a scientist at the Centre for Maritime Research and Experimentation, La Spezia, Italy. **Salvatore Maresca** is a scientist at the Centre for Maritime Research and Experimentation, La Spezia, Italy.

measure hurricane-force ocean surface winds. Thus, the instrument has been mounted on aircraft that typically make butterfly-pattern reconnaissance flights within TCs. In general, SFMR measures the nadir brightness temperatures between 4.5 and 7.2 GHz, which are converted to 1-minute sustained surface wind speeds using a dedicated GMF. Comparison of SFMR to GPS dropsonde wind speed measurements resulted in an error of approximately 4 m s^{-1} in TC winds between 10 and 70 m s^{-1} (Uhlhorn et al., 2007).

Prior to making these comparisons, all SFMR measurements were corrected for the time difference between SAR acquisition and the C-130 flight track. Therefore, every measurement is shifted with respect to the movement of the storm center within the time difference. This results in adjusted flight tracks such that SFMR measurements have the same location with respect to the center of the storm during the SAR acquisition as they actually had when they were recorded. This adjustment does not consider any storm rotation. The storm's movement is derived from the best track information from the Joint Typhoon Warning Center. Figure 1 shows the SAR image of Typhoon Malakas on September 22, 2010, with the original flight track and the superimposed flight track adjusted for the movement of the storm center.

SAR WIND RETRIEVAL

In general, the ability to measure ocean surface winds from spaceborne C-band SAR operating with co-pol is based on the fact that the local wind field generates small-scale ocean surface roughness on horizontal scales of 5–10 cm that increases with wind speed. For radar

backscatter at moderate incident angles (20° to 60°), the NRCS is proportional to the spectral density of the surface roughness on scales comparable to the radar wavelength plus scattering from breaking-water events (Phillips, 1988). In the case of cross-pol, the scattering from surface roughness is significantly smaller and is, in fact, zero for a non-tilted ocean surface (Wright, 1968; Valenzuela, 1978), so the scattering from breaking water dominates the radar cross section for cross-pol (Hwang et al., 2010). Multiple theoretical studies and field experiments show that wave energy dissipation (in the form of breaking) follows a cubic wind-speed dependence (Ochi, 2003; and see Hwang et al., 2010, for a summary of references), so under the very high winds of typhoon conditions, breaking waves will tend to occur uniformly throughout the storm.

Ocean surface wind retrieval from SAR is a two-step process. The first step is to retrieve wind directions, which are a necessary input to the second step. Wind directions can be extracted from

wind-induced streaks visible in the SAR image at different scales. Wind speeds are retrieved from the backscattered NRCS of the ocean surface using a GMF, which describes the dependence of the NRCS on wind and radar imaging geometry.

SAR Wind Direction Retrieval

SAR wind direction retrieval is based on wind-induced phenomena (wind streaks) that are often visible in SAR imagery and aligned in the mean surface wind direction (Gerling, 1986; Wackerman et al., 1996; Lehner et al., 1998). These wind streaks are observed in standard marine radar images and appear to be well aligned (within 13°) to the mean surface wind direction (Dankert and Horstmann, 2007). The orientations of these features can be derived by various methods; this study uses the Local Gradient (LG) method (Horstmann et al. 2002; Horstmann and Koch, 2005). Therefore, the SAR image is smoothed and reduced to resolutions of 100, 200, and 400 m. From each of these

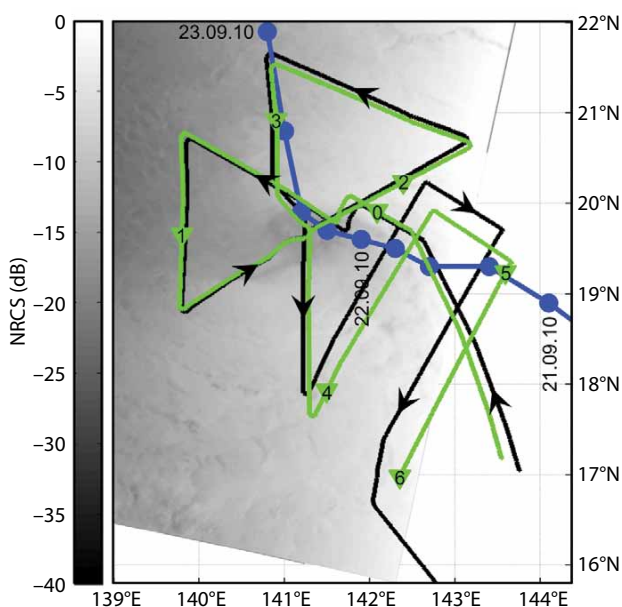


Figure 1. Synthetic aperture radar (SAR) image of Typhoon Malakas acquired by the Canadian satellite RADARSAT-2 on September 22, 2010, at 20:30 UTC using C-band with horizontal polarization in transmit and receive (HH-pol). The black line depicts the original C-130 flight track, and the green line is its correction for SAR image acquisition time. Numbers in the green triangles represent the time difference of the flight track with respect to SAR acquisition. The blue line shows the best track of the typhoon provided by the Joint Typhoon Warning Center.

images, local directions, defined by the normal to the LG, are computed leaving a 180° ambiguity. In the next step, all pixels that are affected by non-wind-induced features, for example, land, surface slicks, and heavy rain, are masked and excluded from further analysis. Therefore, high-resolution land masks and SAR image filters, described by Koch (2004), are considered. The image filters are extracted from the SAR image itself considering locally retrieved parameters, for example, the mean and standard deviation of the image intensity as well as the strength of the retrieved LGs. The most frequent directions in a predefined grid cell (20 km within this investigation) are computed from all the retrieved local directions on the different scales. To remove the remaining directional ambiguities resulting from the various scales, we selected the direction in each grid cell that is closest to circular around the center of the TC eye, assuming a 15° inflow decreasing to a 0° inflow over a distance of 150 km from the TC eye. For grid cells at a greater distance from the TC eye, we selected the nearest direction to its neighboring grid cell (starting from the center of the TC eye).

SAR Wind Speed Retrieval

SAR wind speed retrieval is based on the strong dependence of the NRCS on the local surface wind. This relation is given by GMFs that typically provide the NRCS as a function of the equivalent neutral wind vector at a 10 m anemometer height, incidence angle, wind direction with respect to the radar look direction, radar frequency, and polarization. In the case of SAR data acquired at C-band VV-polarization, there are a number of well-validated model

functions available (Hersbach, 2010). Each of these GMFs is directly applicable for wind-speed retrieval from C-band VV-pol SAR images (Monaldo et al., 2002). For this investigation, we used the CMOD5n GMF, which was carefully evaluated, considering co-located scatterometer NRCS measurements and numerical model winds. However, in the case of SAR data acquired at HH-pol, no similar well-validated GMF exists. To meet this deficiency, we used a hybrid model function that consists of a C-band polarization ratio (PR) and one of the previously mentioned GMFs (Horstmann et al., 2000; Vachon and Dobson, 2000). The PR is defined as the ratio of HH-polarization NRCS to VV-polarization NRCS. The optimal PR value is uncertain and a variety of PRs have been proposed (Thompson et al., 1998; Mouche et al., 2005; Zhang et al., 2011). In this study, we use the PR proposed by Thompson et al. (1998), which neglects wind speed and wind direction dependence but shows good results when used for wind-speed retrieval (Horstmann and Koch, 2005).

For C-band SAR data acquired at cross-pol, several GMFs have been suggested. The GMF that was developed using RADARSAT-2 SAR data acquired at quad-pol (all four polarization pairs) using co-located in situ wind measurements from buoy data of up to 22.5 m s^{-1} is independent from incidence angle and wind direction (Vachon and Wolfe, 2011; Zhang et al., 2011). Recently developed GMFs use RADARSAT-2 ScanSAR cross-pol data with co-located SFMR measurements that show additional dependence on wind direction and incidence angle (van Zedelhoff et al., 2013; recent work of the authors

and colleagues). Within this study, the wind-direction-dependent GMF proposed by the authors was used for all SAR cross-pol data.

Using the approach described above, all wind directions were extracted from the co-pol SAR data on a 20 km grid and extrapolated to a resolution of 1 km. The final resolution of the SAR-retrieved wind speeds is 1 km, retrieved from co-pol as well as cross-pol SAR data using the appropriate GMF.

COMPARISON OF QuikSCAT AND SFMR

We compared the wind fields from RADARSAT-1 SAR co-pol imagery to co-located QuikSCAT wind fields. For this comparison, seven RADARSAT-1 SAR images of TC were available. All images were acquired at HH-pol in the ScanSAR Wide mode A with a time lag of less than 30 minutes relative to QuikSCAT acquisition (Table 1).

Because QuikSCAT operates at Ku-band and is very sensitive to heavy rain, we only considered QuikSCAT data that were not flagged for rain. This significantly reduced the amount of available data, particularly near the storm's core.

Figure 2 shows the RADARSAT-1 ScanSAR image of Typhoon Fitow acquired on August 31, 2007, when it was a category 2 typhoon. Superimposed on the image is the propagation track of the storm as well as wind directions from the SAR image (green arrows) and QuikSCAT data (blue arrows). The regions without wind vectors plotted represent the QuikSCAT data that were flagged for rain. Large rain bands can also be identified in the SAR image of these regions (dark features in the SAR image).

Figure 3 shows the scatter plot of the comparison of QuikSCAT to SAR wind directions (left-hand side) and wind speeds (right-hand side). In these plots, the color-coding is with respect to individual storms, each representing a SAR acquisition. The main statistical parameters for the wind direction retrieval resulted in a correlation of 0.96 with a bias of 6.4° and an rms error of 17.6° . The slight bias indicates a lack of inflow with respect to SAR wind directions, in particular, in the vicinity of the TC eye. Comparisons of wind speeds resulted in a correlation of 0.69 with a bias of 1.34 m s^{-1} and an rms error of 4.55 m s^{-1} , where SAR underestimates wind speeds. Because wind speeds in TCs are highly variable on short spatial scales and RADARSAT ScanSAR wind fields offer a much higher resolution than QuikSCAT, it may not be suitable to use this comparison for validating SAR wind retrieval in the vicinity of the TC eye.

SAR-retrieved wind speeds were compared to SFMR data, which have similar resolution and scales as the SAR wind fields and thus are more representative of the quality of SAR-retrieved wind speeds. For this comparison, SAR data were acquired in the dual-pol mode, resulting in a co-pol and a cross-pol image for each acquisition. For each polarization, wind speeds were retrieved

Table 1. ScanSAR data from RADARSAT-1 and RADARSAT-2 used in this paper, with co-located wind measurements from the Ku-band scatterometer QuikSCAT and the airborne Stepped Frequency Microwave Radiometer (SFMR).

Name of Storm	Image Date and Time (GMT)	Saffir-Simpson Hurricane Scale	Available Wind Measurements
Nockten	Oct 23, 2004, 21:19	3	QuikSCAT
Mawar	Aug 22, 2005, 20:39	4	QuikSCAT
Ewiniar	Jul 3, 2006, 20:54	2	QuikSCAT
Yagi	Sep 21, 2006, 20:18	4	QuikSCAT
Usagi	Aug 1, 2007, 20:58	3	QuikSCAT
Fitow	Aug 31, 2007, 19:43	1	QuikSCAT
Krosa	Oct 4, 2007, 21:34	2	QuikSCAT
Earl	Sep 2, 2010, 22:59	2	SFMR
Fanapi	Sep 13, 2010, 09:09	tropical storm	SFMR
Fanapi	Sep 17, 2010, 21:15	2	SFMR
Malakas	Sep 22, 2010, 20:30	tropical storm	SFMR
Malakas	Sep 24, 2010, 08:45	2	SFMR
Megi	Oct 14, 2010, 09:02	tropical storm	SFMR

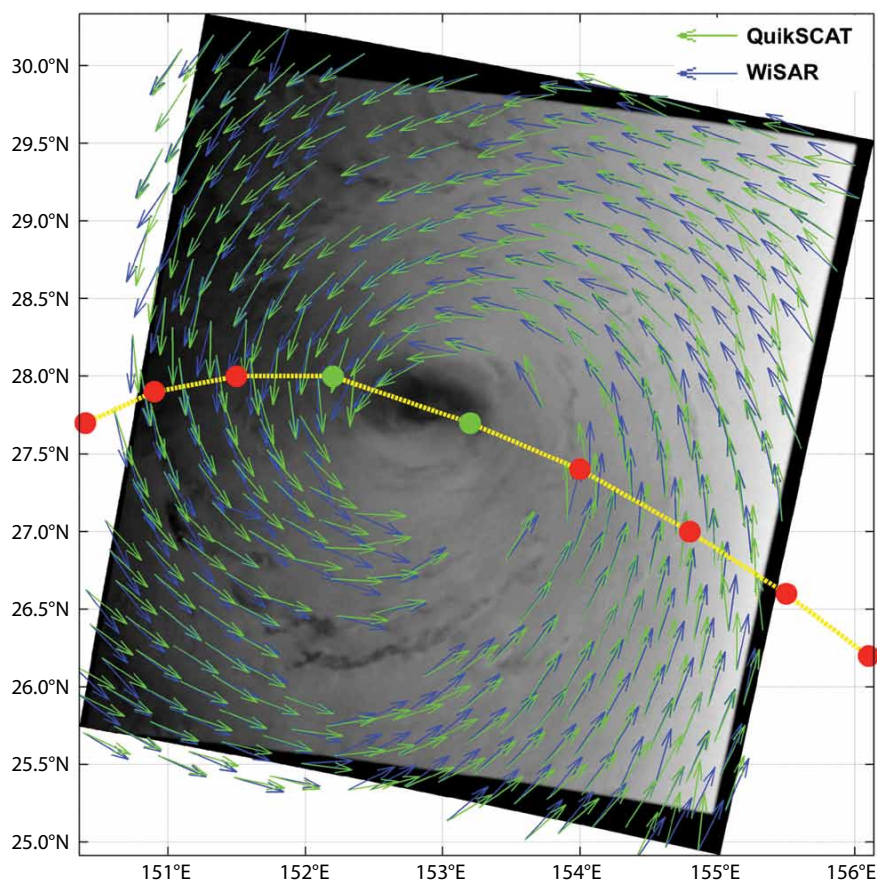


Figure 2. RADARSAT-1 ScanSAR image of Typhoon Fitow acquired on August 31, 2007, at 19:43 UTC. Superimposed on the SAR image are wind directions derived from the SAR image (blue arrows) and from the QuikSCAT data (green arrows). Wind directions are only plotted in the regions that were not flagged for rain in the QuikSCAT data. The best typhoon track data are provided by the Joint Typhoon Warning Center, represented by the yellow line.

using the wind directions resulting solely from the co-pol images.

Figure 4 shows examples of the resulting wind fields from a RADARSAT-2 ScanSAR dual-pol acquisition imaged during Typhoon Malakas on the September 22, 2010, at 20:30 UTC. Malakas formed as a tropical depression on September 20, 2010, and propagated westward. On September 21, it turned into a tropical storm. The storm intensified the next day, and its propagation direction changed to northward toward the Japanese islands just after acquisition of the Figure 1 SAR image. On September 23, the storm became a typhoon, intensifying to category 2 the next day. Finally, the system weakened and transitioned into a powerful extra-tropical cyclone on September 25.

Figure 4 shows the wind fields from the HH-pol data (left) and from the

HV-pol data (right). Corrected SFMR flight tracks, color-coded in accordance with the measured wind speeds, are superimposed on the image. All the white areas in the HV-image represent wind speeds below 10 m s^{-1} where the wind retrieval from RADARSAT-2 ScanSAR cross-pol data is highly uncertain as the expected NRCS is close to the noise floor level of the SAR sensor (recent work of the authors and colleagues). Both wind fields resolve the storm fairly well and also compare fairly well to the SFMR. However, at higher wind speeds, the co-pol retrieved wind speeds deviate significantly from SFMR results, which is due to the very weak dependence of the NRCS on wind speeds over 25 m s^{-1} and, in particular, at low incidence angles ($< 30^\circ$). This behavior is not observed at cross-pol, where the dependence of the NRCS was

observed for wind speeds above 35 m s^{-1} (van Zedelhoff et al., 2013; recent work of the authors and colleagues). The largest differences between SFMR and SAR were observed along the flight track southeast of the typhoon's eye, which is most likely due to the 5 h time difference of the two measurements and the change in the storm's propagation direction (Figure 1). However, the overall comparison of SAR co-pol and cross-pol to SFMR showed better agreement for cross-pol, especially at wind speeds over 20 m s^{-1} .

Figure 5 displays another example of wind fields retrieved from the RADARSAT-2 SAR dual-pol data; they were collected during Hurricane Earl on September 2, 2010, at 22:59 UTC. Earl formed 690 km west of the Cape Verde Islands on August 25, intensified to a tropical storm within hours of genesis,

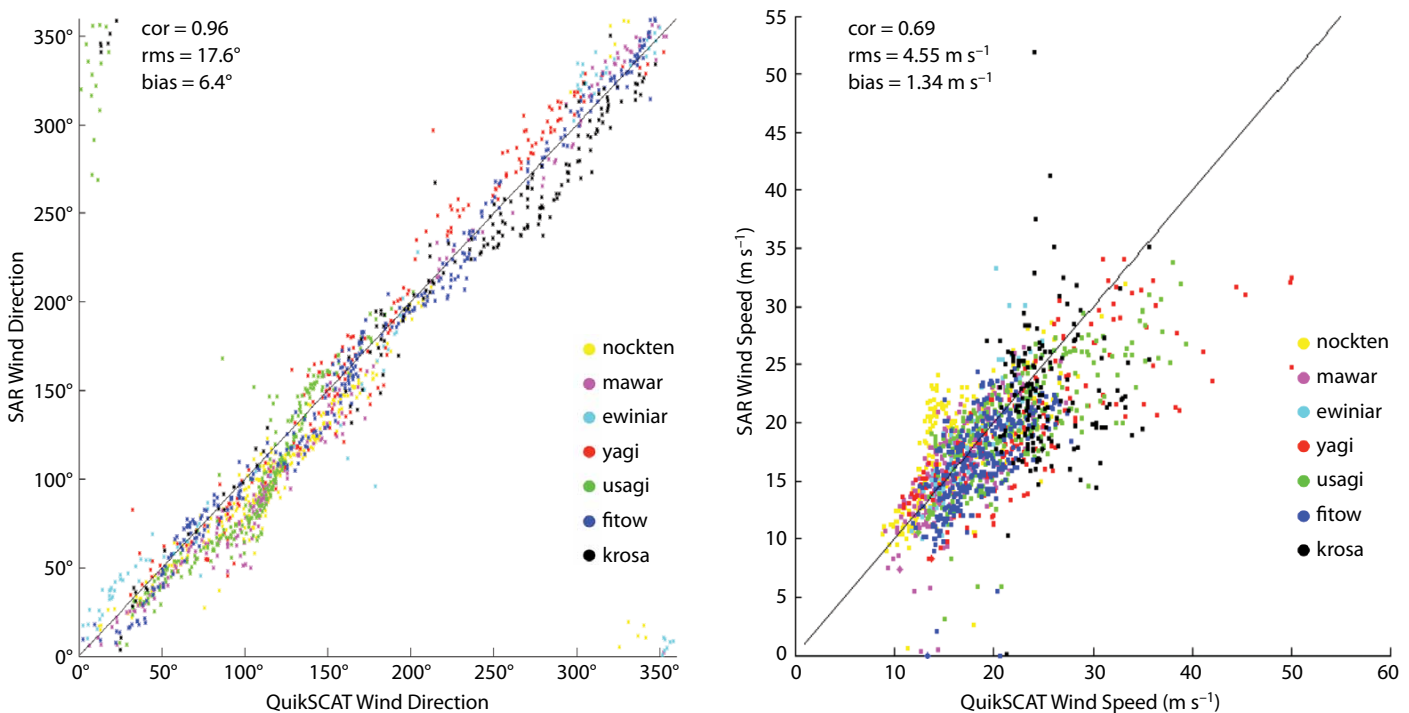


Figure 3. Scatterplots of wind directions (left) and wind speeds (right) showing results from QuikSCAT versus RADARSAT-1 SAR co-pol, acquired at HH-pol.

and propagated westward. On August 29, the storm intensified into a hurricane, and the next day into a major hurricane as it passed the Leeward Islands. On September 2, when a RADARSAT-2 SAR image was acquired, Earl reached its peak intensity as a category 2 hurricane. The next day, the system turned northeast and slowly weakened over decreasing sea surface temperatures, passing approximately 140 km east of Cape Hatteras. Earl accelerated northeastward and made landfall near Western Head, Nova Scotia, traversing the peninsula. Finally, the hurricane transitioned into an extratropical cyclone and was absorbed by a low-pressure system on September 6 north of Newfoundland.

In contrast to the ScanSAR data collected during Typhoon Malakas, the ScanSAR data for Earl were collected using VV-pol and VH-pol. Figure 5 depicts the wind field resulting from VV-pol (left) and from VH-pol (right). As in Figure 4, corrected SFMR flights are superimposed on the wind maps. In case of the co-pol wind field, there is a significant difference between SAR and SFMR wind speeds, in particular, north and south of the storm's eye. This significant underprediction of wind speed both upwind and downwind with respect to the SAR look has been observed by various investigators and is often referred to as the "hour glass effect." Comparison of SAR cross-pol winds to SFMR shows

much better agreement. The main differences are observed west of the storm's eye where cross-pol significantly overestimates wind speeds while co-pol winds are in good agreement. These areas would need to be investigated in greater detail to determine what led to the high backscatter for cross-pol. In general, wind speed retrieval, particularly at high wind speeds, is significantly more accurate using cross-pol data.

In total, six RADARSAT-2 ScanSAR dual-pol data sets were available with co-located SFMR data. To validate the wind retrieval scheme introduced earlier, the SAR-retrieved co-pol and cross-pol wind speeds were compared to SFMR data. In contrast to the comparison to

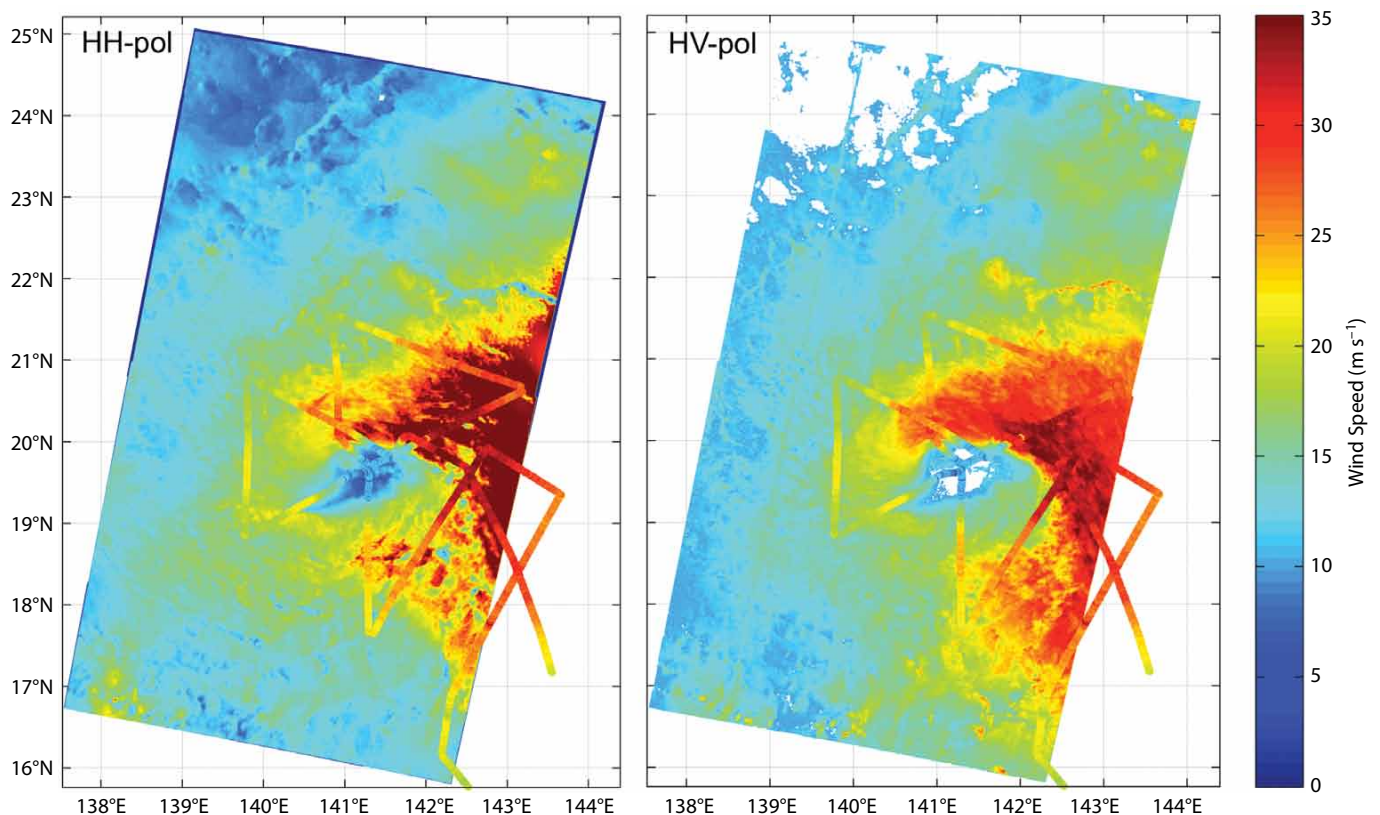


Figure 4. RADARSAT-2 ScanSAR retrieved wind fields for Tropical Storm Malakas acquired on September 22, 2010, at 20:29 UTC at HH-pol (left) and at HV-pol (right). For comparison, wind speed results from Stepped Frequency Microwave Radiometer (SFMR) flights are superimposed on the SAR retrieved winds, which were corrected with respect to the SAR image acquisition time. The flight track color-coding refers to SFMR measured wind speeds.

QuikSCAT data, all points in the SAR co-pol data were excluded that had an NRCS value beyond the definition of the CMOD5n. These points are located in the high-wind-speed regions of the storm at incidence angles below 30° , and they are regions where the co-pol data show a very small dependency of wind speed on the NRCS. In the case of cross-pol retrieved winds, all points were considered in the comparison.

Figure 6 shows scatter plots of the comparison, with the left-hand side displaying the comparison to co-pol and the right-hand side to cross-pol. Within this comparison, each SFMR measurement was compared to the mean wind speed retrieved from all pixels within a range of 2 km of the SFMR location. This comparison was performed because of the highly variable wind speed within the hurricane, the uncertain location of the SFMR measurement due to the

time shift, and tilt and roll of the aircraft. The main statistical parameters for co-pol result in a correlation of 0.77 and an rms error of 5.2 m s^{-1} with a bias of -1.94 m s^{-1} with significant errors at wind speeds above 25 m s^{-1} . In case of cross-pol data, the main statistical parameters result in a correlation of 0.86 and an rms error of 3.8 m s^{-1} with a bias of -0.72 m s^{-1} . The performance of the cross-pol retrieved wind speeds is similar over the entire range of wind speeds, due to the strong wind-speed dependence of the NRCS over the entire range of wind speeds.

Table 2 lists the main statistical parameters for different comparison methods. In the first row, the statistical parameters were computed on the basis of the nearest SAR pixel to an SFMR measurement. They are closest in terms of pixel size, but the comparison suffers due to the time difference between SAR

image acquisition and the SFMR flight, as well as the tilt and roll of the aircraft, which can change the SFMR-imaged swath on the ocean surface. To account for tilt and roll, as well as strong wind variation within the storm, we compared the data from the two sources by searching for the best-agreeing measurement within 2 km of the flight track (2 km jitter). Another method for accounting for these differences in space and time is to consider all pixels within 2 km of the SAR location and retrieve the median (third column) as well as the mean (last column and Figure 6) wind speed and compare them to SFMR measurements. In general, the cross-pol retrieved wind speeds agree with SAR significantly better than SFMR wind speeds, notably at wind speeds above 25 m s^{-1} . The co-pol retrieved wind speeds also have a larger bias as a result of the higher wind-speed regions.

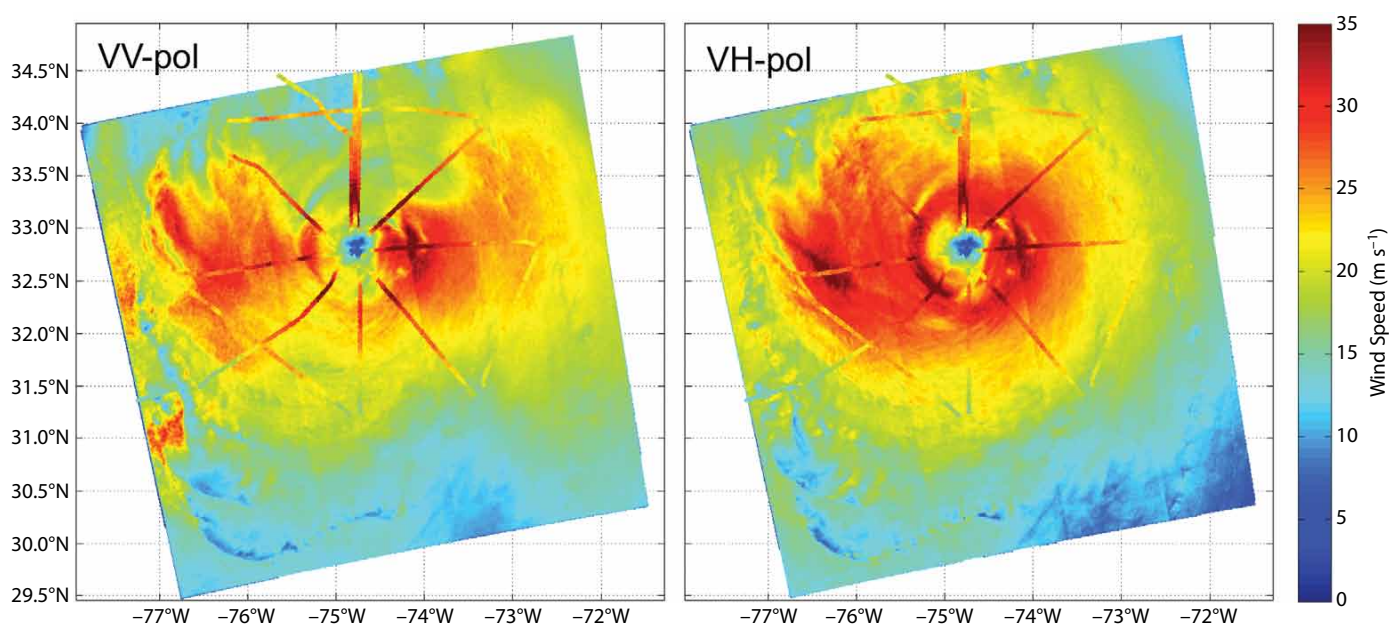


Figure 5. RADARSAT-2 ScanSAR retrieved wind fields for Hurricane Earl acquired on September 2, 2010, at 22:59 UTC at VV-pol (left) and at VH-pol (right). For comparison, wind speed results from SFMR flights are superimposed on SAR-retrieved winds, which were corrected with respect to the SAR image acquisition time. The flight track color-coding refers to SFMR measured wind speeds.

Table 3 compares individual SAR images to SFMR measurements. Within this comparison, the SAR wind speeds resulting from the mean of all SAR pixels within a distance of 2 km of the SFMR location were considered. As in the overall comparison, the cross-pol retrieved SAR winds agree significantly better than the co-pol retrieved wind speeds, in particular, when the storms captured higher wind speeds such during as Earl (September 2), Fanapi (September 13), and Malakas (September 22 and 24) (see also Figure 6).

In the case of lower wind speeds ($< 10 \text{ m s}^{-1}$), ScanSAR cross-pol data are known to be uncertain, as the NRCS from the ocean surface is of the same magnitude as the noise floor of the instrument. However, the noise floor of RADARSAT-2 SAR data varies strongly with different modes and has proven to

be suitable for cross-pol wind retrieval at low wind speeds when using data acquired in quad-pol mode (Vachon and Wolfe, 2011; Zhang et al., 2011).

CONCLUSIONS AND OUTLOOK

This study shows that it is possible to generate useful information about the wind field within a typhoon from SAR imagery in either co-pol or cross-pol modes that could be used to initialize model predictions and potentially generate improved performance. Co-pol imagery is required to estimate wind directions, and, using the local gradient approach, these wind direction estimates have an rms error of 17.6° . There is a slight bias to the SAR-derived wind directions, indicating that they need to be rotated to have more inflow than the SAR image features suggest, which may be due to the time lag required for the

typhoon winds to impact ocean surface features. Typhoon wind speeds can be estimated from either the co-pol or the cross-pol imagery. The cross-pol imagery cannot estimate wind speeds less than 10 m s^{-1} , but its performance improves when estimating wind speeds greater than 25 m s^{-1} . Co-pol imagery can estimate wind speeds less than 10 m s^{-1} , but it shows poorer performance for higher wind speeds. Overall, the co-pol imagery generates wind speed estimates with an rms error of $4.6\text{--}5.2 \text{ m s}^{-1}$, whereas cross-pol imagery rms error is $3.3\text{--}3.8 \text{ m s}^{-1}$. The different error ranges arise from using different methods to compare estimations with in situ observations, taking into account the uncertainty in location from turbulent typhoon winds.

Clearly, having both co-pol and cross-pol SAR imagery collected simultaneously would provide the best range of

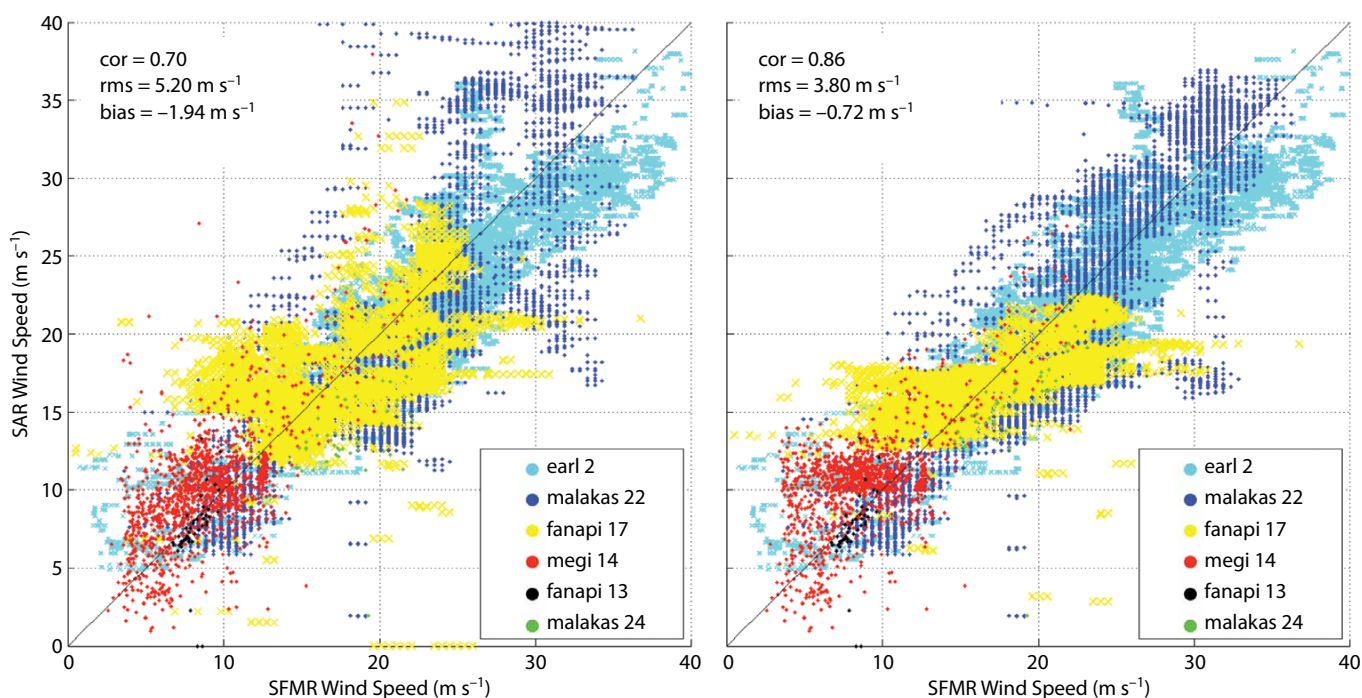


Figure 6. Scatterplot of SFMR wind speed measurements versus SAR retrieved wind speeds resulting from co-pol data (left) and cross-pol data (right). The color-coding represents the different SAR acquisitions.

Table 2. Main statistical parameters resulting from comparison of SAR-retrieved wind speeds to SFMR results, considering different methods for retrieving co-located SAR wind speeds.


	Correlation		Bias (m s ⁻¹)		Standard Deviation (m s ⁻¹)		Root Mean Square Error (m s ⁻¹)	
	Co-pol	Cross-pol	Co-pol	Cross-pol	Co-pol	Cross-pol	Co-pol	Cross-pol
Nearest	0.70	0.86	-1.94	-0.68	4.84	3.71	5.21	3.77
2 km Jitter	0.77	0.89	-1.85	-0.65	4.22	3.22	4.61	3.28
2 km Mean	0.70	0.86	-1.94	-0.72	4.85	3.72	5.22	3.79
2 km Median	0.71	0.86	-1.92	-0.53	4.76	3.67	5.13	3.70

Table 3. Main statistical parameters resulting from comparison of SAR-retrieved wind speeds to SFMR results, considering all SAR images as well as each individual SAR image.

	Correlation		Bias (m s ⁻¹)		Standard Deviation (m s ⁻¹)		Root Mean Square Error (m s ⁻¹)	
	Co-pol	Cross-pol	Co-pol	Cross-pol	Co-pol	Cross-pol	Co-pol	Cross-pol
All images	0.70	0.86	-1.94	-0.72	4.85	3.72	5.22	3.79
Earl Sep 2	0.49	0.84	-4.18	-1.34	5.61	3.19	7.00	3.55
Fanapi Sep 13	0.43	0.41	-0.68	-0.69	2.18	2.16	2.27	2.26
Fanapi Sep 17	0.47	0.49	-0.07	-0.58	4.23	3.81	4.23	3.85
Malakas Sep 22	0.77	0.87	0.51	-0.68	6.77	3.82	6.78	3.88
Malakas Sep 24	0.54	0.55	-4.57	-2.88	2.76	2.68	5.34	3.93
Megi Oct 14	0.66	0.63	1.37	1.60	3.42	2.89	3.68	3.31

information. Future work should examine the best approaches for fusing both wind estimates into a single product. In addition, work is now needed to determine the best approaches for incorporating SAR-derived winds into typhoon models and to determine whether they do, in fact, improve prediction of storm landfall and the storm's strength at that time. This would, of course, be the ultimate application for making the use of SAR imagery important—if it could help save lives and reduce property damage from typhoons.

ACKNOWLEDGEMENTS

We want to thank the Office of Naval Research for supporting this research within the Department Research Initiative on Impacts of Typhoons on the Ocean in the Pacific (ITOP) under Award N0001412WX20895 and Contract N00014-10-C-0317. All RADARSAT-1 and 2 SAR data were kindly made available by M. Caruso of the Center for Southeastern Tropical Advanced Remote Sensing, University of Miami, within the ITOP program. 

REFERENCES

- Chelton, D.B., and M.H. Freilich. 2005. Scatterometer-based assessment of 10-m wind analyses from the operational ECMWF and NCEP numerical weather prediction models. *Monthly Weather Review* 133:409–429, <http://dx.doi.org/10.1175/MWR-2861.1>.
- Dankert, H., and J. Horstmann. 2007. A marine radar wind sensor. *Journal of Atmospheric and Oceanic Technology* 24:1,629–1,642, <http://dx.doi.org/10.1175/JTECH2083.1>.
- Gerling, T. 1986. Structure of the surface wind field from Seasat SAR. *Journal of Geophysical Research* 91:2,308–2,320, <http://dx.doi.org/10.1029/JC091iC02p02308>.
- Hersbach, H. 2010. Comparison of C-Band scatterometer CMOD5.N equivalent neutral winds with ECMWF. *Journal of Atmospheric and Oceanic Technology* 27:721–736, <http://dx.doi.org/10.1175/2009JTECHO698.1>.

- Horstmann, J., and W. Koch. 2005. Measurement of ocean surface winds using synthetic aperture radars. *IEEE Journal of Oceanic Engineering* 30:508–515, <http://dx.doi.org/10.1109/JOE.2005.857514>.
- Horstmann, J., W. Koch, S. Lehner, and R. Tonboe. 2000. Wind retrieval over the ocean using synthetic aperture radar with C-band HH polarization. *IEEE Transactions on Geoscience and Remote Sensing* 38:2,122–2,131, <http://dx.doi.org/10.1109/36.868871>.
- Horstmann, J., W. Koch, S. Lehner, and R. Tonboe. 2002. Ocean winds from RADARSAT-1 ScanSAR. *Canadian Journal of Remote Sensing* 28:524–533, <http://dx.doi.org/10.5589/m02-043>.
- Horstmann, J., D.R. Thompson, F. Monaldo, S. Iris, and H.C. Graber. 2005. Can synthetic aperture radars be used to estimate hurricane force winds? *Geophysical Research Letters* 32, L22801, <http://dx.doi.org/10.1029/2005GL023992>.
- Hwang, P.A., B. Zhang, and W. Perrie. 2010. Depolarized radar return for breaking wave measurements and hurricane wind retrieval. *Geophysical Research Letters* 37, L01604, <http://dx.doi.org/10.1029/2009GL041780>.
- Katsaros, K.B., P.W. Vachon, P.G. Black, P.P. Dodge, and E.W. Uhlhorn. 2000. Wind fields from SAR: Could they improve our understanding of storm dynamics? *Johns Hopkins APL Technical Digest* 21:86–93.
- Katsaros, K.B., P.W. Vachon, W.T. Liu, and P.G. Black. 2002. Microwave remote sensing of tropical cyclones from space. *Journal of Oceanography* 58:137–151, <http://dx.doi.org/10.1023/A:1015884903180>.
- Koch, W. 2004. Directional analysis of SAR images aiming at wind direction. *IEEE Transactions on Geoscience and Remote Sensing* 42:702–710, <http://dx.doi.org/10.1109/TGRS.2003.818811>.
- Lehner, S., J. Horstmann, W. Koch, and W. Rosenthal. 1998. Mesoscale wind measurements using recalibrated ERS SAR images. *Journal of Geophysical Research* 103(C4):7,847–7,856, <http://dx.doi.org/10.1029/97JC02726>.
- Monaldo, F., D. Thompson, R. Beal, W. Pichel, and P. Clemente-Colon. 2002. Comparison of SAR derived wind speed with model predictions and ocean buoy measurements. *IEEE Transactions on Geoscience and Remote Sensing* 39:2,587–2,600, <http://dx.doi.org/10.1109/36.974994>.
- Mouche, A., D. Hauser, J.-F. Daloze, and C. Guerinl. 2005. Dual-polarization measurements at C-band over the ocean: Results from airborne radar observations and comparisons with Envisat Asar data. *IEEE Transactions on Geoscience and Remote Sensing* 43:753–769, <http://dx.doi.org/10.1109/TGRS.2005.843951>.
- Ochi, M.K. 2003. *Hurricane-Generated Seas*. Elsevier Ocean Engineering Book Series, vol. 8, Oxford, UK.
- Phillips, O.M. 1988. Radar returns from the sea surface: Bragg scattering and breaking waves. *Journal of Physical Oceanography* 18:1,065–1,074, [http://dx.doi.org/10.1175/1520-0485\(1988\)018<1065:RRFTSS>2.0.CO;2](http://dx.doi.org/10.1175/1520-0485(1988)018<1065:RRFTSS>2.0.CO;2).
- Reppucci, A., S. Lehner, J. Schulz-Stellenfleth, and S. Brusch. 2010. Tropical cyclone intensity estimated from wide-swath SAR images. *IEEE Transactions on Geoscience and Remote Sensing* 48:1,639–1,649, <http://dx.doi.org/10.1109/TGRS.2009.2037143>.
- Shen, H., Y. He, and W. Perrie. 2009. Speed ambiguity in hurricane wind retrieval from SAR imagery. *International Journal of Remote Sensing* 30:2,827–2,836, <http://dx.doi.org/10.1080/01431160802555879>.
- Thompson, D., T. Elfouhaily, and B. Chapron. 1998. Polarization ratio for microwave backscattering from the ocean surface at low to moderate incidence angles. 1998. Pp. 1,671–1,673 in *Proceedings of the International Geoscience and Remote Sensing Symposium*, 1998, vol. 3. Seattle, WA, USA, <http://dx.doi.org/10.1109/IGARSS.1998.692411>.
- Touzi, R., P.W. Vachon, and J. Wolfe. 2010. Requirement on antenna cross-polarization isolation for the operational use of C-band SAR constellations in maritime surveillance. *IEEE Geoscience and Remote Sensing Letters* 7:861–865, <http://dx.doi.org/10.1109/LGRS.2010.2053835>.
- Uhlhorn, E.W., P.G. Black, J.L. Franklin, M. Goodberlet, J. Carswell, and A.S. Goldstein. 2007. Hurricane surface wind measurements from an operational stepped frequency microwave radiometer. *Monthly Weather Review* 135:3,070–3,085, <http://dx.doi.org/10.1175/MWR3454.1>.
- Vachon, P., and F. Dobson. 2000. Wind retrieval from RADARSAT SAR images: Selection of a suitable C-band HH polarization wind retrieval model. *Canadian Journal of Remote Sensing* 26:306–313.
- Vachon, P., and J. Wolfe. 2011. C-band cross-polarization wind speed retrieval. *IEEE Geoscience and Remote Sensing Letters* 8:456–459, <http://dx.doi.org/10.1109/LGRS.2010.2085417>.
- Valenzuela, G.R. 1978. Theories for the interaction of electromagnetic and oceanic waves – A review. *Boundary-Layer Meteorology* 13:61–85, <http://dx.doi.org/10.1007/BF00913863>.
- van Zadelhoff, G.-J., A. Stoffelen, P.W. Vachon, J. Wolfe, J. Horstmann, and M. Belmonte Rivas. 2013. Scatterometer hurricane wind speed retrievals using cross polarization. *Atmospheric Measurement Techniques Discussions* 6:7,945–7,984, <http://dx.doi.org/10.5194/amtd-6-7945-2013>.
- Wackerman, C., C. Rufenach, R. Schuchman, J. Johannessen, and K. Davidson. 1996. Wind vector retrieval using ERS-1 synthetic aperture radar imagery. *IEEE Transactions on Geoscience and Remote Sensing* 34:1,343–1,352, <http://dx.doi.org/10.1109/36.544558>.
- Wright, J.W. 1968. A new model for sea clutter. *IEEE Transactions Antennas and Propagation* 16(2): 217–223, <http://dx.doi.org/10.1109/TAP.1968.1139147>.
- Zhang, B., W. Perrie, and Y. He. 2011. Wind speed retrieval from RADARSAT-2 quad-polarization images using a new polarization ratio model. *Journal of Geophysical Research* 116, C08008, <http://dx.doi.org/10.1029/2010JC006522>.